ACS OMEGA

http://pubs.acs.org/journal/acsodf

Article

Pyrene-Functionalized Fluorescent Nanojars: Synthesis, Mass Spectrometric, and Photophysical Studies

Melanie M. Mitchell, Vageesha W. Liyana Gunawardana, Guda Ramakrishna,* and Gellert Mezei*

Cite This: *ACS Omega* 2021, 6, 33180−33191

Read Online

ACCESS | Metrics & More | Article Recommendations | Supporting Information

ABSTRACT: Nanojars are a class of supramolecular coordination complexes based on pyrazolate, Cu^{2+}, and OH^- ions that self-assemble around highly hydrophilic anions and serve as efficient anion binding and extraction agents. In this work, the synthesis, characterization, and photophysical properties of pyrene-functionalized fluorescent nanojars are presented. Three pyrene derivatives, 4-(pyren-1-yl)pyrazole (H**L1**), 4-(5-(pyren-1-yl)pent-4-yn-1-yl)-pyrazole (H**L2**), and 4-(3-(pyrazol-4-yl)propyl)-1-(pyren-1-yl)-1,2,3-triazole (H**L3**), and the corresponding nanojars were synthesized and characterized using nuclear magnetic resonance spectroscopy and mass spectrometry. Electronic absorption, steady-state, and time-resolved fluorescence measurements were carried out to understand the interaction between the pyrene fluorophore and copper nanojars. Optical absorption measurements have shown minor ground state interaction between the fluorophore and nanojars. The fluorescence of pyrene is significantly quenched when attached to nanojars, suggesting strong contribution from the paramagnetic Cu^{2+} ions. Significant static quenching is observed in the case of **L1**, when pyrene is directly bound to the nanojar, whereas in the case of **L2** and **L3**, when pyrene is attached to the nanojars using flexible tethers, both static and dynamic quenching are observed.

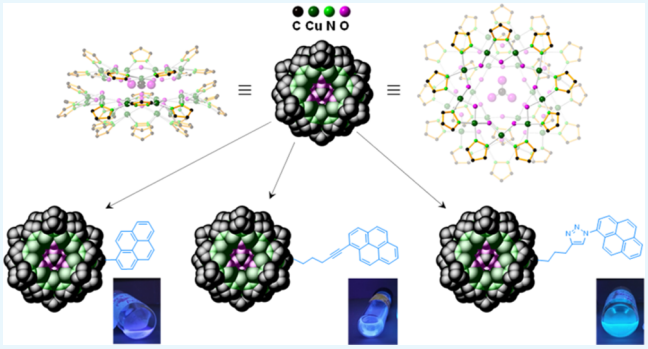

■ INTRODUCTION

Nanojars (NJs) constitute an interesting class of cyclic coordination oligomers based on the neutral {*cis*-Cu^{II}(μ-OH)(μ-pz)} (pz = pyrazolate anion or a derivative) repeating unit (Figure 1).[1] Highly hydrophilic oxyanions, such as carbonate, sulfate, phosphate, and arsenate, template the self-assembly of NJs of the formula [anion⊂{Cu(μ-OH)(μ-pz)}$_n$]$^{2-}$ (Cu_n; n = 26−33).[2−7] Each member of this series of oligomerization isomers is composed of three [{Cu(μ-OH)(μ-pz)}$_m$] (m = 6−14, except 11) metallamacrocycles, strongly held together by an intricate network of hydrogen bonds and Cu···O interactions. As the NJs self-assemble, a hydrophilic cavity lined by a multitude (26−33) of O−H hydrogen bond donors forms at their center, which incarcerates the templating oxyanion. Consequently, NJs have been developed into highly efficient anion-extracting agents,[8] capable of binding trace amounts of oxyanions and transferring even the most hydrophilic ones from water into long-chain aliphatic hydrocarbon solvents.[9] Selective binding of oxyanions has recently been achieved by tethering pairs of pyrazolate ligands together.[10,11]

Aiming at detecting NJs using fluorescence and ultimately developing NJ-based sensors for oxyanions, we pursued the synthesis and characterization of fluorescent NJs. Various polar substituents (including nitro, amine, aldehyde, carboxylate) as well as acidic groups (phenol, thiol, carboxylic acid) interfere with NJ formation. Therefore, we opted for pyrene as the fluorescent label, an aromatic hydrocarbon with no polar or acidic groups yet a very versatile fluorescent moiety. Indeed, pyrene-based fluorescent tags have been used in various coordination complexes,[12] metal−organic frameworks,[13,14] and self-assembled nanomaterials,[15] in fluorescent sensors for the detection of explosives[16] or transition metal ions such as Cu^{2+},[17] Zn^{2+},[18] Hg^{2+},[19] and Fe^{3+},[20] in luminous molecular liquids,[21] surfactant aggregates,[22,23] and dendrimers.[24] Pyrene-based materials are also valuable in organic electronics,[25−28] photoswitchable nonlinear optical[29] and electroluminescent materials,[30] light-harvesting antenna systems,[31−33] photo-initiators of polymerization[34] and other light-induced reactions,[35,36] molecular receptors,[37−40] and electrocatalysis.[41] Pyrene is also used for imaging biological systems[42−45] and for photodynamic therapy.[46] The methods of functionalization of pyrene to prepare luminescent materials have been reviewed.[47] However, very few studies have focused on the

Received: October 8, 2021
Accepted: November 10, 2021
Published: November 22, 2021

ACS Publications

© 2021 The Authors. Published by American Chemical Society

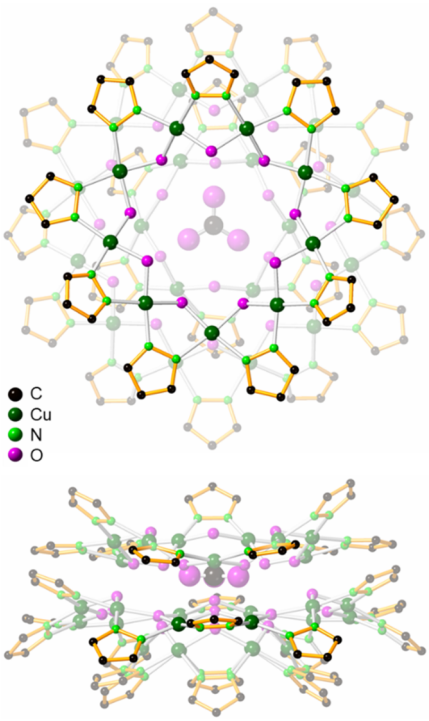

Figure 1. Example of a NJ crystal structure (top- and side-views). Shown here is $[CO_3 \subset \{Cu^{II}(\mu\text{-OH})(\mu\text{-pz})\}_{6+12+9}]^{2-}$ (H-atoms are omitted for clarity).

excited-state interactions between fluorescent dyes and supramolecular inorganic nanomaterials.[48]

Herein, we present the synthesis and characterization of three novel pyrene-functionalized pyrazole ligands, 4-(pyren-1-yl)pyrazole (H**L1**), 4-(5-(pyren-1-yl)pent-4-yn-1-yl)pyrazole (H**L2**), and 4-(3-(pyrazol-4-yl)propyl)-1-(pyren-1-yl)-1,2,3-triazole (H**L3**) (Scheme 1). In H**L1**, the fluorescent tag is directly bound to the pyrazole moiety; therefore, the fluorophore is conjugated with the Cu^{2+} centers in NJs via the pyrazole unit, and its position relative to the NJ is rigid. In contrast, in H**L2** and H**L3**, the fluorescent tag is attached to the pyrazole moiety via a propylene chain (and a −C≡C− or triazole group in H**L2** and H**L3**, respectively), which allows for flexibility of the fluorophore relative to the NJ and disrupts conjugation between the fluorophore and the Cu^{2+} centers. Three different ways of synthesizing fluorescent NJs based on these ligands are described. Electrospray-ionization mass spectrometry (ESI-MS), nuclear magnetic resonance (NMR), optical absorption, steady-state and time-resolved fluorescence measurements were carried out to characterize the novel NJs and to monitor their interaction with the attached pyrene dye.

■ RESULTS AND DISCUSSION

Synthesis of the Fluorescent Pyrazole Ligands. Our previous investigations had established that steric influences from bulky substituents at the 3-position of pyrazole ligands can hinder the self-assembly of NJs, whereas functionalization at the 4-position does not interfere with NJ formation.[9] Thus, the simplest fluorescent pyrazole ligand was synthesized by directly attaching pyrene to the 4-position of the pyrazole moiety (Scheme 1). 4-Pyrazoleboronic acid pinacol ester was first protected with a tetrahydropyranyl (THP) group (Figures S1 and S2), followed by a Suzuki−Miyaura coupling with 1-bromopyrene. The resulting intermediate was deprotected and the product was purified by flash chromatography to give H**L1** in 50% overall yield (Figures S3 and S4).

We were also interested in developing appropriately functionalized pyrazole ligands as an avenue to constructing NJs that have potential to be functionalized both pre- and post-synthetically. We identified 4-(pent-4-yn-1-yl)pyrazole as a suitable starting point for our studies, which combines several desired features: (1) the reactive terminal alkyne functionality allows for the installation of pyrene moieties; (2) the alkyne group is tolerated during NJ self-assembly;[49] (3) the propylene unit between pyrazole and the alkyne prevents π-electron

Scheme 1. Synthesis of the Fluorescent Pyrazole Ligands

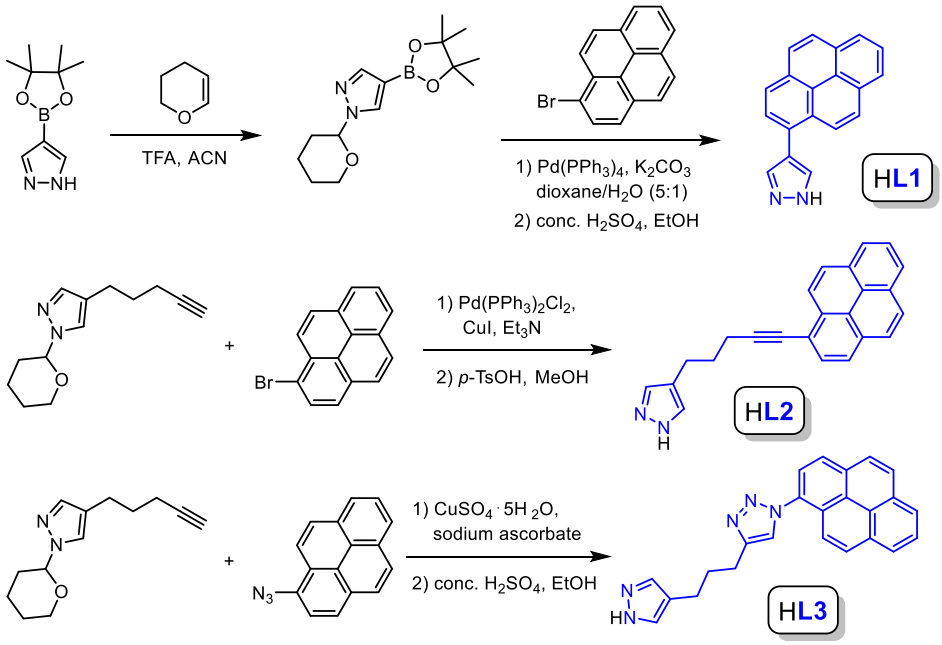

https://doi.org/10.1021/acsomega.1c05619
ACS Omega 2021, 6, 33180−33191

Scheme 2. Different Methods of Synthesizing Fluorescent NJs (Only Cu_{27} is Shown); In Method A, All Pyrazole Moieties of the NJ are Substituted with Pyrene (Only Nine Substituents Are Shown for Clarity); In Method B, NJs with Varying Numbers of Substituents (Depending on the pz/Fluorescent Ligand Ratio) Are Obtained; For Method C, an Example with Two Substituents Is Shown

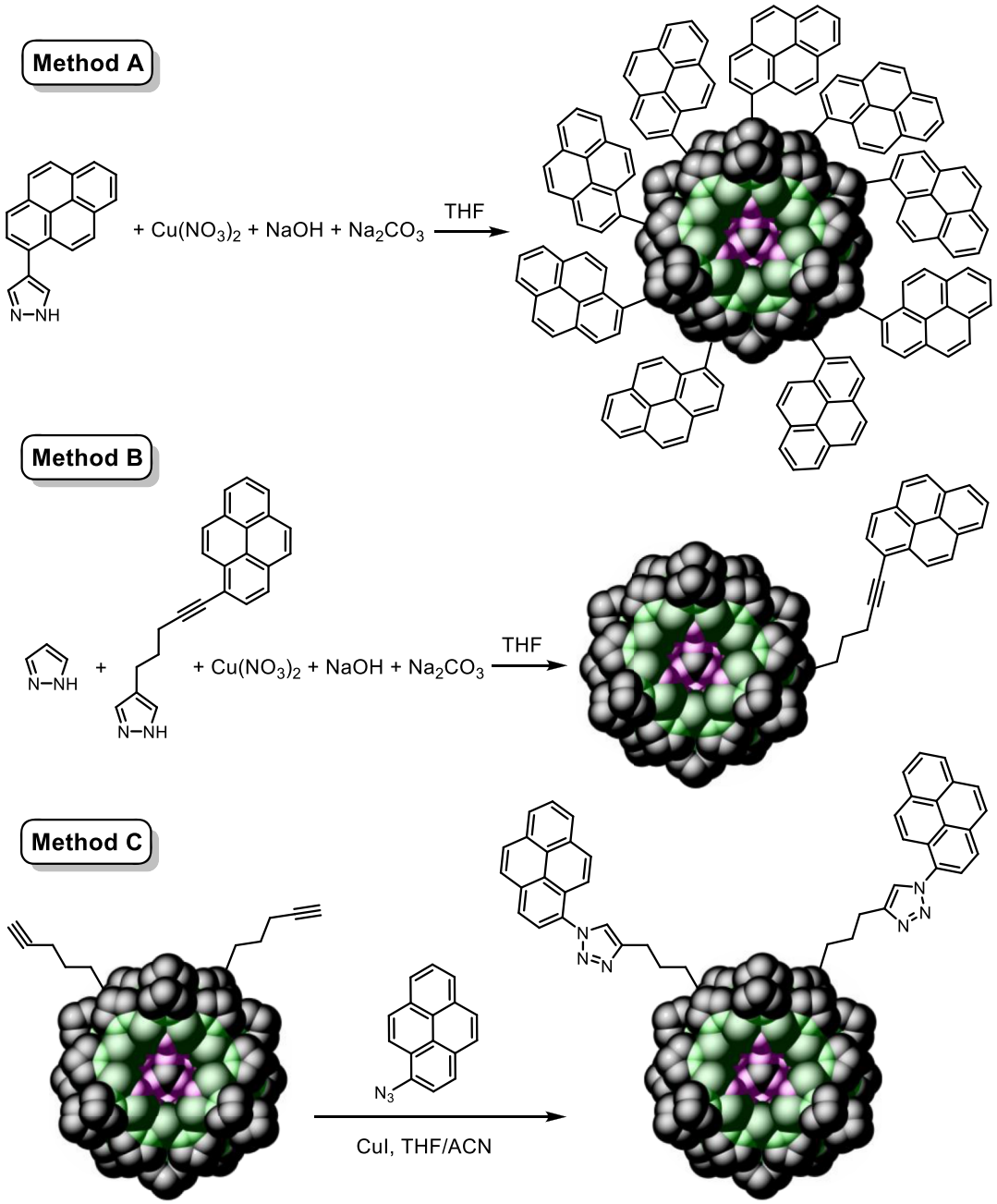

conjugation between the pyrazole and the pyrene moieties, which might lead to diminishing of fluorescence intensity. This compound has been previously prepared from 4-(3-hydroxypropyl)pyrazole by first converting the hydroxyl group to the primary bromide using phosphorus tribromide and subsequently performing a nucleophilic substitution reaction with sodium acetylide to give the alkyne.[49]

A terminal alkyne can be directly coupled to pyrene using a Sonogashira reaction. Thus, a coupling reaction was carried out using the THP-protected 4-(pent-4-yn-1-yl)pyrazole and 1-bromopyrene (Scheme 1). Using $Pd(PPh_3)_4$ as a catalyst produced the desired product along with ∼16% of Glaser-type homocoupled di-alkyne. Replacing the catalyst with $Pd(PPh_3)_2Cl_2$ reduced the amount of the side product to ∼4%. Deprotection and purification by flash chromatography afforded H**L2** in 22% yield over two steps (Figures S5 and S6).

The copper catalyzed azide−alkyne cycloaddition "click" reaction is also a convenient method to install pyrene-based fluorophores on larger molecular structures containing an alkyne functionality. Coupling of THP-protected 4-(pent-4-yn-1-yl)pyrazole with 1-azidopyrene was carried out using click chemistry (Scheme 1). The Cu^+ catalyst was prepared *in situ* by the reduction of Cu^{2+} using sodium ascorbate. The resulting crude product was deprotected using concentrated sulfuric acid in ethanol and the product was purified by dissolving in minimal amount of chloroform and precipitating with hexanes.

https://doi.org/10.1021/acsomega.1c05619
ACS Omega 2021, 6, 33180−33191

Filtration gave the pure H**L3** in 47% yield over two steps (Figures S7 and S8).

Synthesis of Fluorescent NJs by Self-Assembly Using Pyrene-Labeled Pyrazole Ligands. *NJs Based on L1.* The synthesis of homoleptic NJs based solely on a given pyrene-labeled ligand was carried out by self-assembly using a 1:1:2:1 molar mixture of ligand (H**L1**, H**L2**, or H**L3**), $Cu(NO_3)_2$, NaOH, and Na_2CO_3 in tetrahydrofuran (THF) (Scheme 2, Method A). With H**L1**, Cu_{27} and Cu_{29} NJs of the formula $[CO_3\subset\{Cu(OH)(\mathbf{L1})\}_n]^{2-}$ (n = 27, m/z 4726; n = 29, m/z 5074) are observed by ESI-MS(−) (Figure S9). Compared to unsubstituted NJs, the signal intensity of ESI-MS(−) is very weak indicating poor ionization efficiency, attributable to the large size and hydrophobicity of the pyrene-decorated NJs. The ^{1}H NMR spectrum of the NJ mixture displays peaks in the 20−40 ppm window that are consistent with previous observations for NJs.[4,5] The signals of the chemically equivalent pyrazole protons in the 3- and 5-positions of both Cu_{27} (Cu_6+Cu_{12}+Cu_9) and Cu_{29} (Cu_8+Cu_{13}+Cu_8) NJs are significantly downfield shifted compared to free pyrazole, due to the presence of paramagnetic Cu^{2+} ions. The extent of these shifts is temperature-dependent, as confirmed by variable temperature ^{1}H NMR studies in the 25−140 °C range (Figure S10). At 25 °C, the spectrum shows four broad distinguishable peaks at 30.3 (Cu_6-ring), 27.1 (Cu_8-ring), 22.4 (Cu_{12}-ring), and 21.2 ppm (Cu_{13}-ring). Increasing temperatures lead to the sharpening of these peaks as the magnetic moment of the copper complex decreases and reveal a new peak at ∼34.0 ppm (Cu_9-ring) at 50 °C which was too broad to be observable at 25 °C. As in the $[CO_3\subset\{Cu(OH)(pz)\}_n]^{2-}$ (n = 27, 29) NJs studied before,[4,5] the pyrazole protons in the Cu_9-ring of the Cu_{27} NJ are the most sensitive to temperature changes as the corresponding peak shifts upfield by over 5 ppm units on going from 25 to 140 °C in a DMSO-d_6 solution. Meanwhile, the peaks corresponding to the Cu_6- and Cu_{12}-rings of the Cu_{27} NJ, as well as the Cu_8- and Cu_{13}-rings of the Cu_{29} NJ experience much smaller shifts of less than 0.6 ppm units.

Heteroleptic NJs synthesized with a 1:1 molar mixture of pyrazole (Hpz) and fluorescent ligand H**L1** display a statistical distribution of species consisting primarily of Cu_{27} NJs $[CO_3\subset Cu_{27}(OH)_{27}(\mathbf{L1})_x(pz)_{27-x}]^{2-}$ (x = 3−19, m/z 2323−3925), as shown by ESI-MS(−) (Figure S11). The ionization efficiency of these heteroleptic NJs is drastically improved compared to those containing only **L1** as the ligand.

NJs Based on L2. The synthesis of homoleptic NJs based on **L2** proceeded similarly to the one using **L1**. However, these very large and hydrophobic NJs do not ionize sufficiently to be properly characterized by ESI-MS. While some low-intensity peaks could be discerned from the background noise in the expected mass region for the corresponding homoleptic NJs, unequivocal assignments could not be performed. On the other hand, heteroleptic NJs $[CO_3\subset Cu_n(OH)_n(\mathbf{L2})_x(pz)_{n-x}]^{2-}$ (n = 27, x = 4−13, m/z 2556−3754; n = 29, x = 7−12, m/z 3103−3769; n = 31, x = 9−15, m/z 3517−4316) could be observed by ESI-MS(−) if a 1:1 molar mixture of pyrazole and H**L2** was used for the synthesis. In the NJ mixture obtained, Cu_{27} species are the major components; smaller amounts of Cu_{29} and Cu_{31} NJs are also observed (Figure S12). Although the ionization efficiency of these assemblies is significantly less than that of NJs containing only unsubstituted pyrazole, the mass spectrum has a sufficient signal-to-noise ratio to clearly distinguish and identify these species.

NJs Based on L3. Attempts to obtain homoleptic NJs based on **L3** yielded brown, insoluble solids instead of blue-green NJs. The triazole functionality in **L3** is also a possible coordination site for copper which can lead to the formation of coordination polymers. This assumption is consistent with previous studies which showed that NJs do not form with pyrazole ligands containing additional coordinating functional groups.[9] Contrary to **L1** and **L2**, no NJs could be obtained with pyrazole/**L3** mixtures in 1:1 or 6:1 molar ratios. Instead, unidentified copper-containing species with m/z < 1000 were observed in the ESI-MS in both cases. A mixture of pyrazole and **L3** in a 19:1 molar ratio, however, did allow the formation of NJs (Figure S13). Thus, the $[CO_3\subset Cu_n(OH)_n(\mathbf{L3})_x(pz)_{n-x}]^{2-}$ (n = 27, x = 1−4, m/z 2178−2642; n = 31, x = 1−4, m/z 2473−2937) species observed in the corresponding ESI-MS(−) spectrum indicate that **L3** is tolerated on NJs in small numbers (up to four **L3** ligands per NJ). According to the statistical distribution[9,49] of the pyrene-functionalized ligand, unsubstituted NJs are also observed in the mixture.

Synthesis of Fluorescent NJs by "Click" Reaction between Alkyne-Functionalized NJs and 1-Azidopyrene. Post-synthetic functionalization was performed on alkyne-substituted NJs using the Cu^+ catalyzed azide−alkyne Huisgen cycloaddition ("click") reaction.[50,51] In most click reactions, the Cu^+ catalyst is generated *in situ* by reducing Cu^{2+} with an excess of sodium ascorbate. This prevents Glaser-type oxidative homocoupling products of alkynes. To prevent the possible reduction of Cu^{2+} ions in NJs by ascorbate, we opted for the use of CuI as the catalyst. Furthermore, because we had observed that the coupled product (**L3**) is only tolerated on NJs in small amounts, NJs prepared with a 90:10 molar ratio of pyrazole and 4-(pent-4-yn-1-yl)pyrazole were used for this study (Figure S14).

Using THF as a solvent, NJs containing up to three pyrene groups were observed: $[CO_3\subset Cu_n(OH)_n(\mathbf{L3})_x(4\text{-pentynylpyrazole})_y(pz)_{n-x-y}]^{2-}$ (n = 27, x = 1, y = 0−2, m/z 2178−2244; n = 31, x = 1−3, y = 0−2, m/z 2473−2848) (Figure S14b). A significant amount of NJs containing unreacted alkyne moieties remained. To test whether this is due to the poor solubility of CuI in THF, we carried out the reaction in acetonitrile (ACN) which is a good solvent for the catalyst. In this case, a dark-blue precipitate formed in the blue reaction mixture. Its blue color and its solubility in THF suggest that this product consists of NJs with multiple pyrenyl-triazole substituents. The increasing hydrophobicity of the assembly with increasing number of coupled ligands makes them gradually less soluble in ACN. Concomitantly, the mother liquor contained uncoupled NJs and those containing only one **L3** ligand (Figure S14c). In an attempt to prevent the precipitation of the larger assemblies as well as to dissolve the catalyst, we also conducted the reaction in a 1:1 mixture of THF and ACN. Most of the alkyne functionalities have reacted in this case; however, the abundances of the NJs containing pyrene-coupled ligands is lower than expected in the corresponding ESI-MS(−) spectrum, likely due to decreased ionization efficiency of the complexes containing multiple **L3** ligands (Figure S14d). Nevertheless, these experiments clearly demonstrate that NJs can be functionalized post-synthetically.

Synthesis of NJs for Photophysical Studies. Fluorescence studies of NJs were hampered by trace amounts of residual, free fluorescent ligand. Because purification of NJs containing large numbers of fluorescent ligands proved to be

https://doi.org/10.1021/acsomega.1c05619
ACS Omega 2021, 6, 33180−33191

difficult, we employed a mixture of pyrazole (Hpz) and fluorescent ligand (H**L1**, H**L2** or H**L3**) in a 19:1 molar ratio (5 mol % fluorescent ligand) to obtain NJ mixtures free of unbound ligand, suitable for photophysical studies. Because only a small amount of fluorescent dye was employed relative to pyrazole, it was expected that only one or two dye molecules would be present per NJ. The corresponding ESI-MS(−) spectra, shown in Figures S15−S17, confirm the expected results. Some of the NJs in the mixture do not contain any dye, which is typical for mixtures obtained by statistical distribution of ligands.[9,49] Also, in the case of **L2** and **L3**, small amounts of NJs with an additional allyl substituent are observed. This is due to the presence of trace amounts of 4-allylpyrazole byproduct in the 4-(pent-4-yn-1-yl)pyrazole precursor used in the synthesis of **L2** and **L3**. This impurity is very difficult to remove completely, and as shown before, even trace amounts are drastically amplified upon incorporation into large assemblies, such as NJs.[49] Fortunately, the presence of traces of allyl-substituted NJs is not a concern for studying the fluorescence of pyrene-functionalized NJs nor is the presence of unfunctionalized NJs, as neither contain fluorescent moieties. These fluorescent NJ samples, used for the photophysical measurements described below, are denoted **L1**-NJ, **L2**-NJ, and **L3**-NJ.

Photophysical Studies. The main focus of the photophysical studies described below is understanding how the spacing between the fluorophore and the NJ influences the optical properties of the assembly. To that end, photophysical properties of the synthesized fluorophores and NJ-bound fluorophores were studied using electronic absorption, steady-state and time-resolved fluorescence measurements. Figure 2

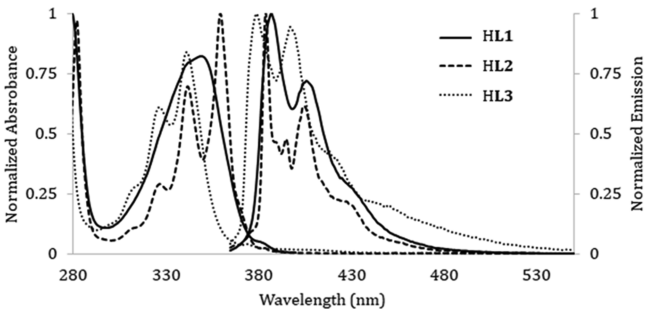

Figure 2. Normalized absorption and fluorescence spectra (after excitation at 350 nm) of the pyrene derivatives H**L1**, H**L2** and H**L3** in ACN (8.4×10^{-6}, 6.0×10^{-6} and 6.4×10^{-6} M, respectively).

shows the normalized absorbance and fluorescence spectra of H**L1**, H**L2** and H**L3** in ACN. The corresponding absorption and fluorescence maxima are presented in Table 1. All synthesized pyrene derivatives have extinction coefficients greater than 10^4 L mol^{-1} cm^{-1}, indicating the $\pi-\pi^*$ nature of the lowest excited state. H**L2** and H**L3** show pronounced vibrational features in their absorption spectra similar to the parent, unsubstituted pyrene molecule, whereas these spectral features are diminished in H**L1**. The absorption maximum of H**L3** (341 nm) is close to that of pyrene (343 nm), whereas the ones of H**L1** and H**L2** are shifted to 349 and 359 nm, respectively. The red shifted absorptions suggest extended conjugation in the latter molecules.

Table 1. Photophysical Properties of the Synthesized Pyrene Derivatives

system	λ_{abs}^{max} (nm)	λ_{em}^{max} (nm)	quantum yield
HL1	349	388	0.26
HL2	359	381	0.08
HL3	341	385	0.085

All three pyrene derivatives show a vibrational structure in their fluorescence spectra and the fluorescence maxima are near 385 nm. Fluorescence quantum yields were determined using 1,4-bis(2-methylstyryl)benzene as standard and are provided in Table 1. H**L1** shows a fluorescence quantum yield of 0.26 while diminished fluorescence quantum yields were observed for H**L2** and H**L3** indicating the presence of faster non-radiative deactivation pathways in these systems.

Figure 3A shows the absorption spectra of H**L1** and **L1**-NJ (prepared as described above). Also, shown in this figure is the absorption spectrum of the non-functionalized NJ based on the parent pyrazole ligand (denoted pz-NJ), which displays the same absorbance maximum at 600 nm as the dye-functionalized NJ. An increased absorbance below 400 nm is observed for **L1**-NJ, indicating the contribution of **L1**. The absorption of **L1** attached to the NJ was determined by subtracting the absorption spectrum of pz-NJ from the one of **L1**-NJ and is shown in the inset of Figure 3A. It is apparent that the absorption spectrum of **L1** slightly broadened when bound to the NJ, indicating electronic interaction between **L1** and the NJ. Similar analyses were carried out for **L2** (Figure 3B) and **L3** (Figure 3C). In these latter cases, the results indicate a negligible ground state interaction between pyrene and NJs, and the vibrational features of pyrene are retained even when the dyes are bound to the NJ. These result are in agreement with the fact that the dyes are tethered to the NJ by spacers that prevent through-bond electronic coupling.

To probe the excited state interaction between pyrene and NJ, steady-state fluorescence measurements were carried out. Figure 4A shows the fluorescence spectra of H**L1** and **L1**-NJ dissolved in ACN. The fluorescence of **L1**-NJ was corrected for the absorbance of **L1** on the NJ. It is evident that the fluorescence of **L1** is quenched 6.3-fold upon binding to the NJ. The inset of Figure 4A shows the normalized fluorescence spectra of **L1** and **L1**-NJ. No noticeable shift in the fluorescence spectrum of **L1** is observed except that there is a strong fluorescence quenching. Similar analyses were carried out for **L2** (Figure 4B) and **L3** (Figure 4C). Again, the fluorescence of the dyes is significantly quenched (25- and 19-fold for **L2** and **L3**, respectively), while only slight changes are observed in the features of the fluorescence spectra. The observed fluorescence quenching is explained by the proximity of the fluorophore to the paramagnetic Cu^{2+} ions in the NJ. However, it is interesting to note that the fluorescence quenching is significantly greater for **L2** and **L3** than for **L1**, which is directly bound to the NJ. This indicates that in addition to enhanced intersystem crossing, dynamic quenching is also present. To rule out the presence of free pyrene dyes in solution and to prove that quenching is associated solely with pyrenes bound to NJs, fluorescence measurements were carried out on 1-bromopyrene at increasing concentrations of pz-NJs (Figure S18). No fluorescence quenching was observed even at significantly elevated concentrations of pz-NJs, confirming that the quenching is arising only when the pyrene is bound to the NJ. Also, to verify that the fluorescence of the dyes is restored when the NJ is broken down, fluorescence measurements were carried out on the synthesized dye-NJ

https://doi.org/10.1021/acsomega.1c05619
ACS Omega 2021, 6, 33180−33191

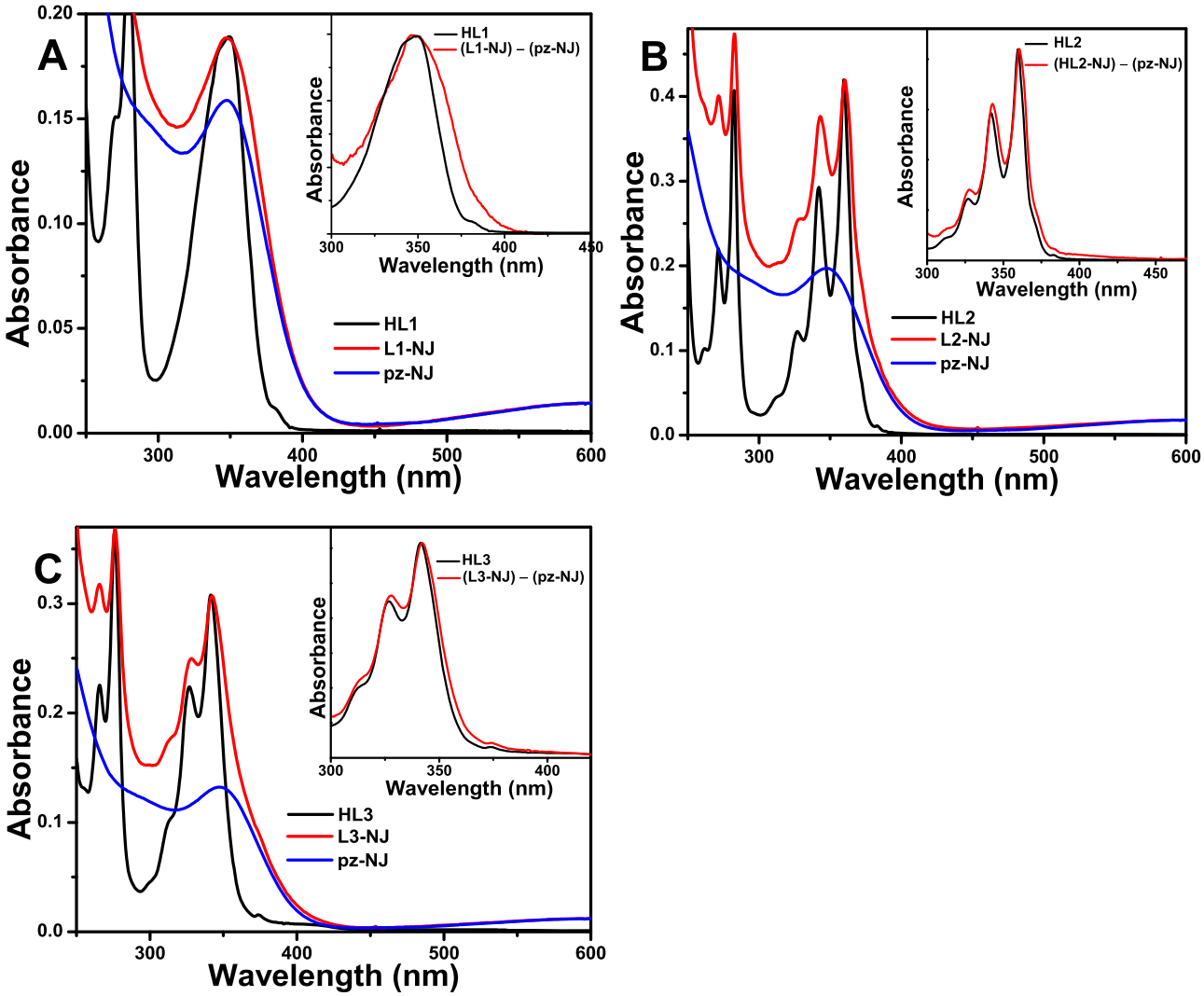

Figure 3. Optical absorption spectra in ACN of free and NJ-bound dyes (A) **L1**, (B) **L2** and (C) **L3** (5.9×10^{-6}, 8.4×10^{-6} and 6.4×10^{-6} M, respectively), along with the absorption spectrum of pz-NJ without dye. Spectra of the free dye and pz-NJ were normalized to that of the NJ-bound dye at 600 nm. Insets show the absorbance of the free dye compared to the one of the NJ-bound dye (determined by subtracting the absorbance of the pz-NJ).

systems in THF solution with increasing amounts of acid. Our previous studies have shown that in the presence of 100 equivalents of acid, pz-NJs are completely broken down. As expected, the fluorescence of the dyes is restored close to the value of the free dye in the presence of 100 equiv of acid (Figure S19).

To understand the mechanism of fluorescence quenching in pyrene-bound NJs, time-resolved fluorescence measurements were carried out using time-correlated single photon counting. The free dyes and NJ-bound dyes were excited with a 373 nm diode and fluorescence of pyrene was monitored at 400 nm. Parts A, B, and C of Figure 5 show the comparative decay traces for H**L1**, H**L2**, H**L3** and the corresponding NJs, respectively. The fluorescence decay of pyrene is faster when bound to NJs than in the free form in solution. A significantly faster decay was observed for **L2** and **L3** bound to the NJs, compared to **L1**. Fluorescence lifetimes were determined by fitting the decay traces to a multi-exponential decay function and the obtained lifetime data are provided in Table 2. Two decay components were obtained for H**L1** in ACN with lifetimes of 2.1 ns (3.3%) and 11.7 ns (96.7%). An average lifetime was determined using the equation $\tau_{avg} = \sum a_i\tau_i / \sum a_i$, which provides a value of 11.4 ns for H**L1**. For **L1**-NJ, the decay is again fit to a double exponential function providing an average lifetime of 10.9 ns. The decrease in fluorescence lifetime is marginal in the case of **L1**-NJ, suggesting that the observed steady-state quenching is mostly static in nature. In contrast, the fluorescence decay of **L2** was fit with two lifetime components of 3.2 ns (19.6%) and 14.4 ns (80.4%) and an average lifetime of 12.2 ns was obtained. However, the decay of **L2**-NJ is much faster than that of H**L2** and triple exponential decay was needed to fit the decay. An average lifetime of 4.4 ns is determined for **L2**-NJ indicating that the fluorescence quenching has contributions from dynamic quenching. Similarly, a decreased average lifetime of 5.4 ns was obtained for **L3**-NJ when compared to H**L3** (13.3 ns). The varying photoluminescence quenching observed for the different pyrene derivatives bound to copper NJs is likely related to the distance between fluorophore and NJ, as well as to the orientation of the fluorophore on the NJs. Additionally, through-bond vs. through-space fluorescence quenching needs to be considered in these systems.

https://doi.org/10.1021/acsomega.1c05619
ACS Omega 2021, 6, 33180−33191

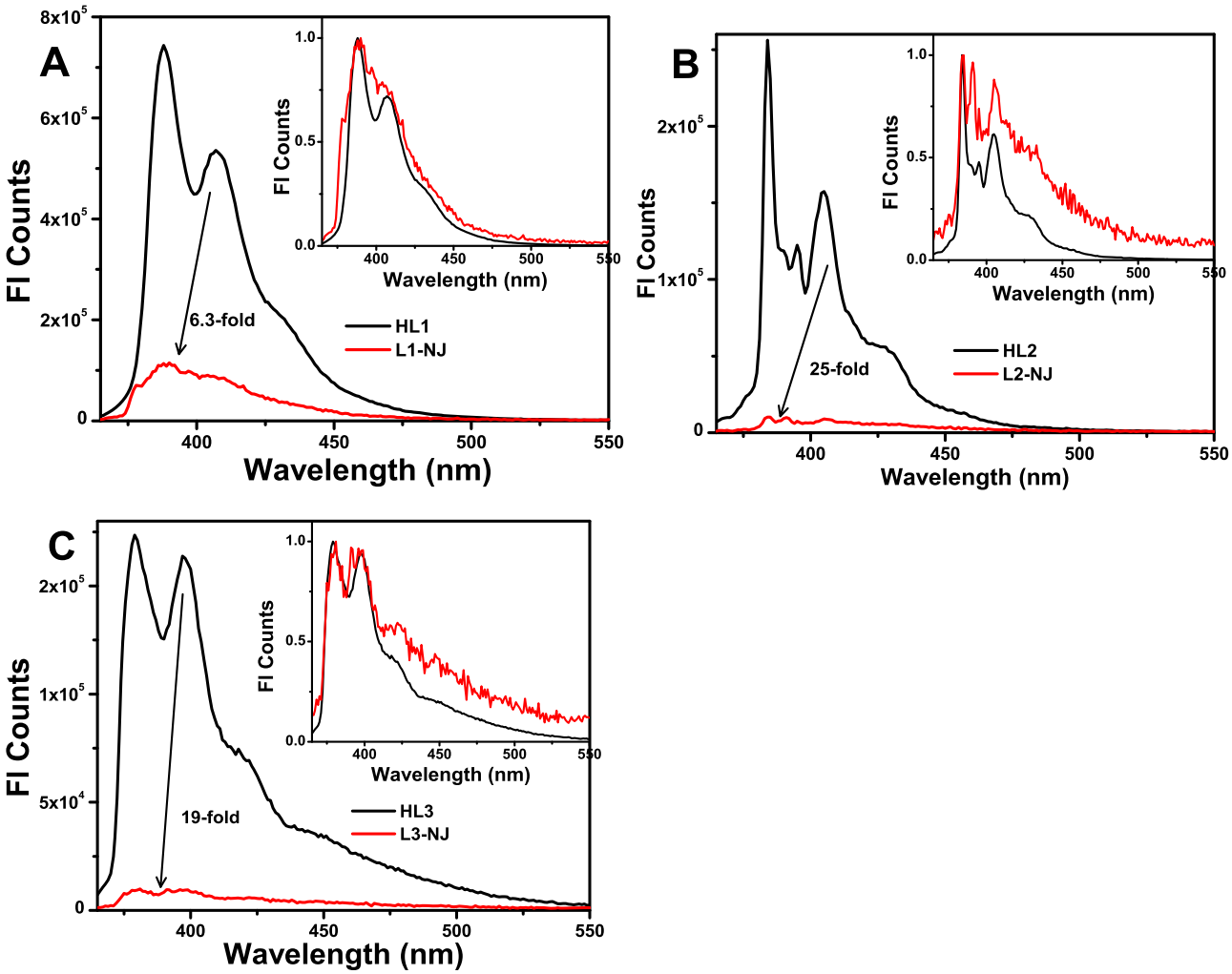

Figure 4. Steady-state fluorescence spectra after excitation at 350 nm of free pyrene ligands (8.4×10^{-6}, 6.0×10^{-6} and 6.4×10^{-6} M, respectively) and NJ-bound ligands (5.9×10^{-6}, 8.4×10^{-6} and 6.4×10^{-6} M, respectively) in ACN for (A) **L1**, (B) **L2** and (C) **L3**. Insets show the normalized fluorescence spectra of free pyrene ligands and NJ-bound ligands.

A 6.3-fold steady-state fluorescence quenching is observed for **L1**-NJ, which is much smaller than the corresponding quenching for **L2**-NJ (25-fold) and **L3**-NJ (19-fold). Due to the structure of the tether, through-bond fluorescence quenching is only possible in the case of **L1**-NJ. Surprisingly, **L1**-NJ shows the least fluorescence quenching among the fluorescent NJ systems studied, despite the fact that the pyrene moiety is the closest to the paramagnetic Cu^{2+} centers in **L1**-NJ. Time-resolved fluorescence measurements have shown little to no decrease in lifetime for **L1**-NJ, while 2.7- and 2.4-fold lifetime quenching is observed for **L2**-NJ and **L3**-NJ, respectively. The fact that the lifetime change is negligible for **L1**-NJ indicates that most of the fluorescence quenching in this system is static in nature, with increased inter-system crossing as the pyrene is closer to the paramagnetic copper centers in the NJ. Additional fluorescence lifetime quenching is observed for **L2**-NJ and **L3**-NJ indicating a contribution of dynamic quenching. The dynamic quenching contribution is likely arising from the fact that **L2** and **L3** possess flexible aliphatic tethers that allow for a closer contact between the pyrene chromophore and the NJ. Current time-resolved fluorescence measurements with limited time resolution (~1 ns) are unable to capture faster deactivation pathways that are apparent in pyrene-bound NJs. Therefore, ultrafast time-resolved measurements are needed on these systems, which will be addressed in upcoming studies.

■ CONCLUSIONS

In summary, three novel pyrene-functionalized pyrazole ligands (H**L1**, H**L2**, and H**L3**) as well as the corresponding NJs containing these fluorescent ligands were synthesized and characterized using NMR spectroscopy, mass spectrometry, and photophysical techniques. Steady-state fluorescence measurements indicate strong and varied fluorescence quenching for these ligands when bound to NJs. With **L1**, where the pyrene fluorophore is directly bound to the copper NJ, a 6.3-fold quenching was observed, whereas with **L2** and **L3** the quenching is 25- and 19-fold, respectively. Time-resolved fluorescence measurements have shown only static quenching for **L1**-NJ, while significant contribution from dynamic quenching is observed for **L2**-NJ and **L3**-NJ. The additional dynamic quenching has origins in the flexibility of **L2** and **L3** which allows for the pyrene moiety to fold back onto the NJs. Because Cu^{2+} is the only metal ion that can be used for the preparation of NJs, future studies will focus on the attachment of the fluorophore using rigid, non-conjugated tethers, which will minimize fluorescence quenching caused by the paramagnetic Cu^{2+} ions.

https://doi.org/10.1021/acsomega.1c05619
ACS Omega 2021, 6, 33180−33191

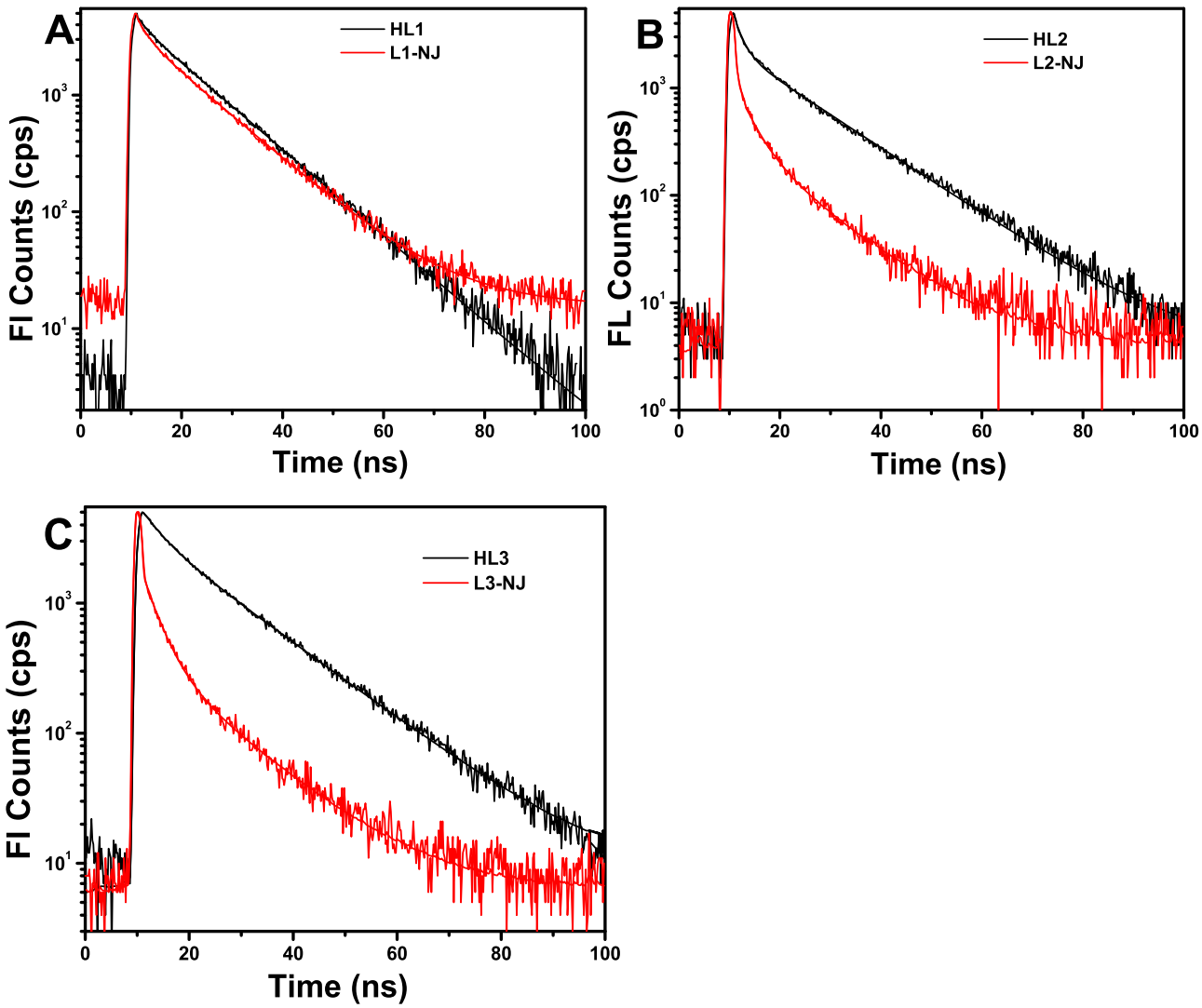

Figure 5. Fluorescence kinetic decay traces for the free dye and NJ-bound dye in ACN at 400 nm for (A) **L1**, (B) **L2** and (C) **L3** after excitation at 370 nm.

Table 2. Fluorescence Lifetimes of the Synthesized Pyrene Derivatives and the Corresponding NJs

system	lifetimes (ns)	average lifetime (ns)
HL1	2.1 ± 0.2 (3.3%), 11.70 ± 0.04 (96.7%)	11.4
L1-NJ	2.0 ± 0.1 (6.8%), 11.60 ± 0.06 (93.2%)	10.9
HL2	3.24 ± 0.08 (19.6%), 14.4 ± 0.1 (80.4%)	12.2
L2-NJ	0.34 ± 0.04 (49.0%), 3.5 ± 0.2 (22.9%), 12.1 ± 0.1 (28.1%)	4.40
HL3	3.4 ± 0.1 (12.0%), 14.60 ± 0.08 (88.0%)	13.3
L3-NJ	0.14 ± 0.04 (32.4%), 3.0 ± 0.1 (33.3%), 12.8 ± 0.1 (34.3%)	5.4

■ EXPERIMENTAL SECTION

General. All reagents used were purchased from commercial sources and were used as received, unless otherwise specified. Solvents were also used as received, except in the synthesis of $Pd(PPh_3)_2Cl_2$, for which THF was dried using sodium/benzophenone, and in the transformation of THP-protected 4-(3-bromopropyl)pyrazole to the corresponding alkyne, for which DMF was dried over 4 Å molecular sieves. Standard Schlenk techniques were used for reactions sensitive to air and/or moisture, and degassing of solvents was performed using the freeze−pump−thaw method. Water was deionized and solvents used for mass spectrometry were mass spectrometry-grade.

1-Bromopyrene,[52] 1-azidopyrene,[53] $Pd(PPh_3)_2Cl_2$,[54] $(Bu_4N)_2[CO_3\{Cu(OH)(pz)\}_n]$ (n = 27, 29−31; pz-NJs),[4] and a mixture of heteroleptic NJs based on a 9:1 molar ratio of pyrazole/4-(pent-4-yn-1-yl)pyrazole were synthesized according to literature procedures.[49] Synthesis of the THP-protected 4-(4-pentynyl)pyrazole (in 5 steps) was also conducted according to referenced procedures,[49] with additional details and adjustments explained herein. In the final step going from the THP-protected 4-(3-bromopropyl)pyrazole to the alkyne product, fresh sodium acetylide (NaC≡CH) slurry was used and 2.65 equiv (of pure sodium acetylide, i.e., not the slurry mixture) were used in the reaction instead of 1.5 equiv listed in the original procedure. All reagents for this final reaction were added under inert atmosphere via syringe. For column chromatography, a ratio of 2.5:1 hexanes/ethyl acetate was used instead of the 2:1 ratio to improve separation and reduce band overlap between the alkyne and the allyl side product within the column. The first fractions of organic material to leave the column contain mostly the allyl impurity, and latter

https://doi.org/10.1021/acsomega.1c05619
ACS Omega 2021, 6, 33180−33191

fractions contain the desired alkyne with increasing purity. The impure fractions are purified in a second column using the same solvent mixture listed here to yield THP-protected 4-(4-pentynyl)pyrazole (yield of crude product: 83.3%; yield of purified product: 45%).

Mass spectrometry was performed using a Waters Synapt G1 HDMS instrument with electrospray ionization (ESI). The settings used for mass spectrometry were as follows: capillary voltage of 2.5 kV, sampling cone voltage of 40 V, extraction cone voltage of 2.5 V, source temperature of 80 °C, desolvation temperature of 110 °C, cone N_2 flow rate of 45 L/h, desolvation N_2 flow rate of 470 L/h. Samples were infused at 5 μL/min. All samples analyzed with the mass spectrometer were dissolved in ACN. ^{1}H NMR spectra were collected using a Jeol JNM-ECZS (400 MHz) spectrometer.

Steady-state ultraviolet−visible (UV−vis) and fluorescence spectra were collected using a Shimadzu UV-1650PC UV−visible spectrophotometer and a Horiba Jobin Yvon FluoroMax-3, respectively. All UV−vis measurements were obtained at 25 °C. Slit widths of excitation and emission were both 1 nm unless otherwise specified. Time-resolved fluorescence measurements were taken on an Edinburgh Instruments F900 spectrofluorometer, equipped with an 800-B pulsed diode laser as the excitation source emitting an excitation wavelength of 373 nm. Time-resolved fluorescence measurements were analyzed with the Edinburgh-Instruments analysis software utilizing either reconvolution or tail-fits.

Synthesis of 1-(Tetrahydro-2*H*-pyran-2-yl)pyrazole-4-boronic Acid Pinacol Ester. Pyrazole-4-boronic acid pinacol ester (1.50 g, 7.73 mmol), ACN (20 mL), 3,4-dihydro-2*H*-pyran (776 μL, 715 mg, 8.51 mmol), and trifluoroacetic acid (50.0 μL, 74.5 mg, 0.653 mmol) were combined in a 50 mL round bottom flask and the solution was refluxed under stirring overnight. After cooling to room temperature, the reaction mixture was quenched with saturated $NaHCO_3$ solution until pH ≈ 8 was reached. The resulting mixture was extracted with dichloromethane (30 mL × 3) and the combined organic layers were dried over anhydrous Na_2SO_4. After filtration, the solvent was removed under reduced pressure yielding 1.90 g of an orange oil that solidified upon standing (yield: 89%). ^{1}H NMR (400 MHz, $CDCl_3$): δ 7.91 (s, 1H, 5-*H*-pz), 7.80 (s, 1H, 3-*H*-pz), 5.38 (dd, 1H, C*H*-THP, J = 9 Hz, 3 Hz), 4.02 (d, 1H, CH_2O-THP, J = 10 Hz), 3.67 (td, 1H, CH_2O-THP, J = 11 Hz, 3 Hz), 1.92−2.20 (m, 3H, CH_2-THP), 1.52−1.77 (m, 3H, CH_2-THP), 1.28 (s, 12H, CH_3) ppm. ^{13}C NMR (101 MHz, $CDCl_3$): δ 145.5, 134.8, 87.4, 67.8, 30.6, 25.0, 24.9, 24.8, 22.4 ppm. HRMS (ESI-TOF) m/z: $[M + Na]^+$ calcd for $C_{14}H_{23}BN_2O_3Na$, 300.1736; found, 300.1754.

Synthesis of 4-(Pyren-1-yl)pyrazole (HL1). In a round-bottom Schlenk flask fitted with a septum, 1-(tetrahydro-2*H*-pyran-2-yl)pyrazole-4-boronic acid pinacol ester (1.53 g, 5.5 mmol) and 1-bromopyrene (1.95 g, 6.95 mmol) were added. The flask was purged with N_2(g) and a degassed mixture of dioxane and water (5:1, 15 mL) was added via syringe. K_2CO_3 (2.93 g, 21.2 mmol) was added, followed by $Pd(PPh_3)_4$ (0.460 g, 0.40 mmol). The walls of the flask were rinsed with the dioxane solution, and a condenser was fitted. The reaction mixture was refluxed under inert atmosphere overnight. Water was added to the red solution, and the product was extracted with ethyl acetate (80 mL × 2). The combined organics were washed with brine (40 mL) and dried over Na_2SO_4. After filtration, the solvent was removed under reduced pressure.

The crude product was dissolved in a 1:50 mixture of dichloromethane and ethanol (100 mL). Concentrated sulfuric acid (5.5 mL) was added dropwise and the reaction was vigorously stirred for 24 h. The reaction was quenched with $NaHCO_3$ to a pH of ∼8. The product was extracted with chloroform (80 mL × 2), and the organic phase was washed with water and brine followed by drying over Na_2SO_4, filtration and removal of solvent under reduced pressure. The crude product (2.63 g) was purified by flash chromatography on silica gel using a 2:1 mixture of ethyl acetate and hexanes (R_f = 0.36) to yield 702 mg of a yellow solid (yield: 48%). Using a 1:1 molar ratio of the pinacol ester starting material and 1-bromopyrene produces a 50% overall yield.[49] ^{1}H NMR (400 MHz, DMSO-d_6): δ 8.44 (d, 1H), 8.26−8.31 (m, 4H), 8.16−8.20 (m, 3H), 7.90−8.10 (m, 3H) ppm. ^{13}C NMR (101 MHz, DMSO-d_6): δ 139.7, 131.6, 131.1, 130.0, 129.4, 128.9, 128.2, 128.1, 128.0, 128.0, 127.5, 126.9, 125.7, 125.3, 124.9, 124.7, 120.2 ppm. HRMS (ESI-TOF) m/z: $[M - H]^-$ calcd for $C_{19}H_{11}N_2$, 267.0922; found, 267.0952.

Synthesis of 4-(5-(Pyren-1-yl)pent-4-yn-1-yl)pyrazole (HL2). The THP-protected pentynyl-pyrazole (320 mg, 1.47 mmol) was added to a 50 mL Schlenk flask. 1-Bromopyrene (414 mg, 1.47 mmol) was added, followed by $PdCl_2(PPh_3)_2$ (110 mg, 0.16 mmol). Triethylamine (12 mL) was added to the flask and the mixture was purged with nitrogen while stirring. CuI (3 mg, 0.016 mmol) was added to the flask and stirred at 65 °C overnight using an oil bath. The deep red/brown mixture was cooled to room temperature and filtered. The flask was rinsed with EtOAc, which was filtered and combined with the previous filtrate. Then, the solvent was removed under reduced pressure yielding 669 mg of crude product, which was dissolved with minimal methanol. *p*-Toluene sulfonic acid monohydrate (608 mg) was added to the solution until a pH of 3 and was stirred for two days. The mixture was quenched with saturated $NaHCO_3$ solution to a pH of ∼8, then extracted with chloroform (100 mL × 3). The combined organics were dried over Na_2SO_4 and the solvent was removed under reduced pressure. The residue was dry loaded onto a silica column and purified with flash chromatography (3:2 EtOAc/hexanes) to yield 115 mg of an orange oil. A second column was performed on impure fractions using 49:1 $CHCl_3$/MeOH to yield an additional 30 mg of H**L2** (overall yield: 30%). ^{1}H NMR (400 MHz, $CDCl_3$): δ 8.56 (d, 1H), 7.99−8.21 (m, 8H), 7.52 (s, 2H), 2.83 (t, 2H, J = 8 Hz), 2.69 (t, 2H, 8 Hz), 2.04 (m, 2H, 7 Hz) ppm. ^{13}C NMR (101 MHz, $CDCl_3$): δ 133.0, 131.9, 131.4, 131.2, 130.8, 129.7, 128.2, 127.9, 127.3, 126.2, 125.7, 125.5, 124.6, 124.5, 120.3, 118.8, 95.7, 80.3, 30.2, 23.4, 19.4 ppm.

Synthesis of 4-(3-(Pyrazol-4-yl)propyl)-1-(pyren-1-yl)-1,2,3-triazole (HL3). 4-(4-Pentyn-1-yl)-1-(tetrahydro-2*H*-pyran-2-yl)pyrazole (270 mg, 1.24 mmol) and 1-azidopyrene (303 mg, 1.25 mmol) were dissolved in degassed THF (15 mL) in an oven-dried 2-neck Schlenk round-bottom flask fitted with a septum. The flask was purged with N_2(g). A solution of $CuSO_4{\cdot}5H_2O$ (463 mg, 1.86 mmol) in H_2O (10 mL) was transferred to the reaction vessel via syringe. A fresh solution of sodium ascorbate in H_2O (15 mL), prepared from ascorbic acid (1.31 g, 7.44 mmol) and $NaHCO_3$ (625 mg, 7.44 mmol), was added dropwise. The walls of the flask were rinsed with THF and the reaction mixture was stirred at room temperature under inert atmosphere for three days. The deep red/brown solution was quenched to neutral pH with NH_4OH (30% wt) solution. The mixture was extracted with chloroform (50 mL ×

https://doi.org/10.1021/acsomega.1c05619
ACS Omega 2021, 6, 33180−33191

4), and the combined organics were washed with H_2O (60 mL × 2) and brine (120 mL). The organic layer was dried over $MgSO_4$, then it was filtered and the solvent was removed by evaporation. The residue was dissolved in EtOH (50 mL) and concentrated sulfuric acid was added dropwise via pipette until the solution had a pH of 3. This reaction mixture was stirred overnight, then was quenched with saturated $NaHCO_3$ solution to a pH of 8. The mixture was extracted with chloroform (60 mL × 3), and the combined organics were washed with H_2O (120 mL × 2) and brine (120 mL × 2). The organic layer was dried over Na_2SO_4, filtered, and concentrated. The resulting red/brown solid was dissolved in a minimal amount of chloroform, and excess diethyl ether was added while mixing to form a brown precipitate. The precipitate was filtered and washed with diethyl ether. Residual solvent was removed from the precipitate under reduced pressure to yield 241 mg of H**L3**. Evaporating the filtrate followed by dissolving the residue in chloroform and precipitating with ether yielded an additional 16 mg of H**L3** (overall yield: 55%). ^{1}H NMR (400 MHz, DMSO-d_6): δ 8.57 (s, 1H, triazole-*H*), 8.49−8.18 (m, 8H, pyrene-*H*), 7.80 (d, 1H, pyrene-*H*, J = 9 Hz), 7.51 (br, 2H, 3,5-*H*-pz), 2.85 (t, 2H, C pz-CH_2CH_2, J = 7 Hz), 2.60 (t, 2H, CH_2CH_2C, J = 7 Hz), 2.02 (m, 2H, $CH_2CH_2CH_2$) ppm. ^{13}C NMR (101 MHz, DMSO-d_6): δ 147.8, 132.1, 131.3, 131.2, 130.7, 130.1, 129.3, 127.7, 127.1, 126.7, 125.9, 125.7, 125.7, 124.6, 124.4, 123.9, 121.7, 119.8, 31.1, 25.2, 23.8 ppm. HRMS (ESI-TOF) m/z: $[M + Na]^+$ calcd for $C_{24}H_{19}N_5Na$, 400.1538; found, 400.1533.

Synthesis of Fluorescent NJs. All NJs in this study were synthesized by standard procedures[4] with details mentioned here. The fluorescent ligand (0.05 mmol) was combined with pyrazole (0.95 mmol) in a 1:19 ratio, respectively, to total 1 mmol in a round bottom flask. $Cu(NO_3)_3{\cdot}2.5H_2O$ (1 mmol) was added, followed by THF (10 mL). NaOH pellets (2.13 mmol) were ground with a mortar and pestle, then added to the THF solution. $Na_2CO_3{\cdot}H_2O$ (1 mmol) was added to the dissolved mixture, capped, and stirred at room temperature for three days. The blue solution was then filtered, and the solvent allowed to evaporate. The residue was redissolved in THF and filtered into a clean beaker to evaporate once more, yielding a blue solid.

The blue NJ solids were dissolved in minimal ACN and stirred for 1 h. This solution was added dropwise to isopropyl ether (threefold excess) and stirred for an additional 30 min. After filtration, a dark-colored residue remained on the filter medium. The solvent was removed under reduced pressure, yielding clean NJs without any free fluorescent dyes (verified with fluorescence spectroscopy).

Click coupling reactions were conducted in degassed solvent and were stirred for 5 days under N_2. 0.1155 g NJ and 1-azidopyrene (0.0359 g) were dissolved in either THF (15 mL), ACN (10 mL), or a mixture of THF/ACN (1:1 v/v, 20 mL). A stock solution of CuI was prepared with 0.0791 g of CuI dissolved in 10 mL of ACN. 710 μL of this solution was added to the reaction mixture and was stirred in the dark.

Titration of 1-Bromopyrene with $(Bu_4N)_2[CO_3\{Cu(OH)(pz)\}_n]$ (n = 27, 29−31; pz-NJs). Solutions of 1-bromopyrene (3.20 μM) and pz-NJs (4.11 μM) were prepared in ACN and were both measured to have an absorbance of 0.12 at 345 nm. Before any titrant was added, the absorbance and emission spectra of the 1-bromopyrene solution (3 mL) was collected as a baseline. 50 μL of the NJ solution was then added to the cuvette containing the analyte, and the absorbance and emission spectra were collected again. This process was repeated in 50 μL additions until a total of 1 mL of NJ solution was added to the cuvette (1 cm path length). The emission spectra were obtained by exciting the solution at 345 nm and monitoring the fluorescence from 360 to 550 nm (using a 5 nm slit width setting).

Titration of L1-NJ, L2-NJ and L3-NJ with Acid. Nitric acid was selected as a titrant because the nitrate ion is known not to interfere with NJs even at high concentrations. Two separate solutions were prepared using a serial dilution method to yield 0.038 M and 0.001 M HNO_3 in THF. A 14 μM **L1**-NJ solution was prepared in THF (10 mL). The absorbance and emission spectra of the **L1**-NJ solution was collected. Two equivalents of HNO_3 (i.e., 279 μL of 0.001 M nitric acid solution) were then added to the **L1**-NJ solution, and the absorbance and emission spectra were collected. This step was repeated after adding additional amounts of acid. Thus, fluorescence spectra were collected for **L1**-NJs with 0, 2, 10, 20, and 100 equiv of HNO_3, indicating an increase in fluorescence intensity with increasing acid equivalents. Each solution was excited at 350 nm and the fluorescence was monitored from 365 to 550 nm (slit widths 5 and 2.5 nm for excitation and emission, respectively). Similar procedures were employed using **L2**-NJ (8.8 μM in THF) and **L3**-NJ (2.3 μM in THF).

■ ASSOCIATED CONTENT

Supporting Information

The Supporting Information is available free of charge at https://pubs.acs.org/doi/10.1021/acsomega.1c05619.

^{1}H NMR, ESI-MS(−), absorbance and fluorescence spectra (PDF)

■ AUTHOR INFORMATION

Corresponding Authors

Gellert Mezei − *Department of Chemistry, Western Michigan University, Kalamazoo, Michigan 49008, USA;* orcid.org/0000-0002-3120-3084; Email: gellert.mezei@wmich.edu

Guda Ramakrishna − *Department of Chemistry, Western Michigan University, Kalamazoo, Michigan 49008, USA;* orcid.org/0000-0002-5288-8780; Email: rama.guda@wmich.edu

Authors

Melanie M. Mitchell − *Department of Chemistry, Western Michigan University, Kalamazoo, Michigan 49008, USA*

Vageesha W. Liyana Gunawardana − *Department of Chemistry, Western Michigan University, Kalamazoo, Michigan 49008, USA*

Complete contact information is available at: https://pubs.acs.org/10.1021/acsomega.1c05619

Notes

The authors declare no competing financial interest.

■ ACKNOWLEDGMENTS

This material is based on work supported by the National Science Foundation under grant no. CHE-1808554.

REFERENCES

(1) Mezei, G.; Baran, P.; Raptis, R. G. Anion Encapsulation by Neutral Supramolecular Assemblies of Cyclic Cu^{II} Complexes: A Series of Five Polymerization Isomers, $[\{cis\text{-}Cu^{II}(\mu\text{-OH})(\mu\text{-pz})\}_n]$, n = 6, 8, 9, 12, and 14. *Angew. Chem., Int. Ed.* **2004**, *43*, 574−577.

(2) Fernando, I. R.; Surmann, S. A.; Urech, A. A.; Poulsen, A. M.; Mezei, G. Selective Total Encapsulation of the Sulfate Anion by Neutral Nano-Jars. *Chem. Commun.* **2012**, *48*, 6860−6862.

(3) Mezei, G. Incarceration of One or Two Phosphate or Arsenate Species within Nanojars, Capped Nanojars and Nanohelicages: Helical Chirality from Two Closely-Spaced, Head-to-Head PO_4^{3-} or AsO_4^{3-} Ions. *Chem. Commun.* **2015**, *51*, 10341−10344.

(4) Ahmed, B. M.; Szymczyna, B. R.; Jianrattanasawat, S.; Surmann, S. A.; Mezei, G. Survival of the Fittest Nanojar: Stepwise Breakdown of Polydisperse Cu_{27}−Cu_{31} Nanojar Mixtures into Monodisperse $Cu_{27}(CO_3)$ and $Cu_{31}(SO_4)$ Nanojars. *Chem.—Eur. J.* **2016**, *22*, 5499−5503.

(5) Ahmed, B. M.; Hartman, C. K.; Mezei, G. Sulfate-Incarcerating Nanojars: Solution and Solid-State Studies, Sulfate Extraction from Water, and Anion Exchange with Carbonate. *Inorg. Chem.* **2016**, *55*, 10666−10679.

(6) Ahmed, B. M.; Mezei, G. From Ordinary to Extraordinary: Insights into the Formation Mechanism and pH-Dependent Assembly/Disassembly of Nanojars. *Inorg. Chem.* **2016**, *55*, 7717−7728.

(7) Hartman, C. K.; Mezei, G. Mapping the Intricate Reactivity of Nanojars toward Molecules of Varying Acidity and Their Conjugate Bases Leading To Exchange of Pyrazolate Ligands. *Inorg. Chem.* **2017**, *56*, 10609−10624.

(8) Mezei, G. Selective Extraction of Anions from Solutions. U.S. Patent 9,901,901 B2, Feb 27, 2018, and 10,087,197 B2 (Oct. 2, 2018); European Patent 2852558 B1 (Sept. 9, 2020).

(9) Ahmed, B. M.; Calco, B.; Mezei, G. Tuning the Structure and Solubility of Nanojars by Peripheral Ligand Substitution, Leading to Unprecedented Liquid−Liquid Extraction of the Carbonate Ion from Water into Aliphatic Solvents. *Dalton Trans.* **2016**, *45*, 8327−8339.

(10) Ahmed, B. M.; Mezei, G. Accessing the Inaccessible: Discrete Multinuclear Coordination Complexes and Selective Anion Binding Attainable Only by Tethering Ligands Together. *Chem. Commun.* **2017**, *53*, 1029−1032.

(11) Al Isawi, W. A.; Salome, A. Z.; Ahmed, B. M.; Zeller, M.; Mezei, G. Selective Binding of Anions by Rigidified Nanojars: Sulfate vs. Carbonate. *Org. Biomol. Chem.* **2021**, *19*, 7641−7654.

(12) Howarth, A. J.; Majewski, M. B.; Wolf, M. O. Photophysical Properties and Applications of Coordination Complexes Incorporating Pyrene. *Coord. Chem. Rev.* **2015**, *282*−*283*, 139−149.

(13) Kinik, F. P.; Ortega-Guerrero, A.; Ongari, D.; Ireland, C. P.; Smit, B. Pyrene-Based Metal Organic Frameworks: From Synthesis to Applications. *Chem. Soc. Rev.* **2021**, *50*, 3143−3177.

(14) Liu, X. T.; Wang, K.; Chang, Z.; Zhang, Y. H.; Xu, J.; Zhao, Y. S.; Bu, X. H. Engineering Donor−Acceptor Heterostructure Metal−Organic Framework Crystals for Photonic Logic Computation. *Angew. Chem., Int. Ed.* **2019**, *58*, 13890−13896.

(15) He, P.-P.; Li, X.-D.; Wang, L.; Wang, H. Bispyrene-Based Self-Assembled Nanomaterials: In Vivo Self-Assembly, Transformation, and Biomedical Effects. *Acc. Chem. Res.* **2019**, *52*, 367−378.

(16) Shanmugaraju, S.; Mukherjee, P. S. π-Electron Rich Small Molecule Sensors for the Recognition of Nitroaromatics. *Chem. Commun.* **2015**, *51*, 16014−16032.

(17) Kowser, Z.; Rayhan, U.; Akther, T.; Redshaw, C.; Yamato, T. A Brief Review on Novel Pyrene Based Fluorometric and Colorimetric Chemosensors for the Detection of Cu^{2+}. *Mater. Chem. Front.* **2021**, *5*, 2173−2200.

(18) Wang, F.; Wang, K.; Kong, Q.; Wang, J.; Xi, D.; Gu, B.; Lu, S.; Wei, T.; Chen, X. Recent Studies Focusing on the Development of Fluorescence Probes for Zinc Ion. *Coord. Chem. Rev.* **2021**, *429*, 213636.

(19) Naskar, B.; Dhara, A.; Modak, R.; Maiti, D. K.; Prodhan, C.; Chaudhuri, K.; Requena, A.; Cerón-Carrasco, J. P.; Goswami, S. A Pyrene-Pyrazole-Based Rotamer Senses Hg^{2+} on the Nanomolar Scale. *ChemistrySelect* **2017**, *2*, 2512−2519.

(20) Chakraborty, S.; Mandal, M.; Rayalu, S. Detection of Iron(III) by Chemo and Fluoro-Sensing Technology. *Inorg. Chem. Commun.* **2020**, *121*, 108189.

(21) Lu, F.; Nakanishi, T. Solvent-Free Luminous Molecular Liquids. *Adv. Optical Mater.* **2019**, *7*, 1900176.

(22) Qiao, M.; Fan, J.; Ding, L.; Fang, Y. Fluorescent Ensemble Sensors and Arrays Based on Surfactant Aggregates Encapsulating Pyrene-Derived Fluorophores for Differentiation Applications. *ACS Appl. Mater. Interfaces* **2021**, *13*, 18395−18412.

(23) Piñeiro, L.; Novo, M.; Al-Soufi, W. Fluorescence Emission of Pyrene in Surfactant Solutions. *Adv. Colloid Interface Sci.* **2015**, *215*, 1−12.

(24) Qiu, J.; Hameau, A.; Shi, X.; Mignani, S.; Majoral, J. P.; Caminade, A. M. Fluorescent Phosphorus Dendrimers: Towards Material and Biological Applications. *ChemPlusChem* **2019**, *84*, 1070−1080.

(25) Figueira-Duarte, T. M.; Müllen, K. Pyrene-Based Materials for Organic Electronics. *Chem. Rev.* **2011**, *111*, 7260−7314.

(26) Poriel, C.; Rault-Berthelot, J. Blue Single-Layer Organic Light-Emitting Diodes Using Fluorescent Materials: A Molecular Design View Point. *Adv. Funct. Mater.* **2020**, *30*, 1910040.

(27) Zhang, K.; Wang, T.; Wu, T.; Ding, Z.; Zhang, Q.; Zhu, W.; Liu, Y. An Effective Strategy to Obtain Near-Infrared Emission from Shoulder to Shoulder-Type Binuclear Platinum(II) Complexes Based on Fused Pyrene Core Bridged Isoquinoline Ligands. *J. Mater. Chem. C* **2021**, *9*, 2282−2290.

(28) Islam, M. M.; Hu, Z.; Wang, Q.; Redshaw, C.; Feng, X. Pyrene-Based Aggregation-Induced Emission Luminogens and their Applications. *Mater. Chem. Front.* **2019**, *3*, 762−781.

(29) Xue, X.; Wang, H.; Han, Y.; Hou, H. Photoswitchable Nonlinear Optical Properties of Metal Complexes. *Dalton Trans.* **2018**, *47*, 13−22.

(30) Ran, H.; Zhao, Z.; Duan, X.; Xie, F.; Han, R.; Sun, H.; Hu, J.-Y. Blue-Emitting Butterfly-Shaped Donor−Acceptor Type 1,3,5,9-Tetraarylpyrenes: Easily Available, Low-Cost Conventional Fluorophores for High-Performance Near Ultraviolet Electroluminescence with $CIE_y < 0.05$. *J. Mater. Chem. C* **2021**, *9*, 260−269.

(31) Pyo, K.; Xu, H.; Han, S. M.; Saxena, S.; Yoon, S. Y.; Wiederrecht, G.; Ramakrishna, G.; Lee, D. Synthesis and Photophysical Properties of Light-Harvesting Gold Nanoclusters Fully Functionalized with Antenna Chromophores. *Small* **2021**, *17*, 2004836.

(32) Cicchi, S.; Fabbrizzi, P.; Ghini, G.; Brandi, A.; Foggi, P.; Marcelli, A.; Righini, R.; Botta, C. Pyrene-Excimers-Based Antenna Systems. *Chem.—Eur. J.* **2009**, *15*, 754−764.

(33) Ensslen, P.; Wagenknecht, H.-A. One-Dimensional Multichromophor Arrays Based on DNA: From Self-Assembly to Light-Harvesting. *Acc. Chem. Res.* **2015**, *48*, 2724−2733.

(34) Dumur, F. Recent Advances on Pyrene-Based Photoinitiators of Polymerization. *Eur. Polym. J.* **2020**, *126*, 109564.

(35) Offenloch, J. T.; Gernhardt, M.; Blinco, J. P.; Frisch, H.; Mutlu, H.; Barner-Kowollik, C. Contemporary Photoligation Chemistry: The Visible Light Challenge. *Chem.—Eur. J.* **2019**, *25*, 3700−3709.

(36) Xiao, P.; Zhang, J.; Zhao, J.; Stenzel, M. H. Light-Induced Release of Molecules from Polymers. *Prog. Polym. Sci.* **2017**, *74*, 1−33.

(37) Manandhar, E.; Wallace, K. J. Host−Guest Chemistry of Pyrene-Based Molecular Receptors. *Inorg. Chim. Acta* **2012**, *381*, 15−43.

(38) Dumitrescu, D. G.; Feng, W.-X.; Legrand, Y.-M.; van der Lee, A.; Petit, E.; Barboiu, M. Pyrene-Box Capsules for Adaptive Encapsulation and Structure Determination of Unstable or Non-crystalline Guest Molecules. *CrystEngComm* **2018**, *20*, 261−270.

(39) Yazaki, K.; Catti, L.; Yoshizawa, M. Polyaromatic Molecular Tubes: From Strategic Synthesis to Host Functions. *Chem. Commun.* **2018**, *54*, 3195−3206.

https://doi.org/10.1021/acsomega.1c05619
ACS Omega 2021, 6, 33180−33191

(40) Ronson, T. K.; Meng, W.; Nitschke, J. R. Design Principles for the Optimization of Guest Binding in Aromatic-Paneled $Fe^{II}_4L^6$ Cages. *J. Am. Chem. Soc.* **2017**, *139*, 9698−9707.
(41) Milton, R. D.; Wang, T.; Knoche, K. L.; Minteer, S. D. Tailoring Biointerfaces for Electrocatalysis. *Langmuir* **2016**, *32*, 2291−2301.
(42) Lee, H. J.; Kim, B. H. Pyrene-Modified Guanine Cluster Probes Forming DNA/RNA Hybrid Three-Way Junctions for Imaging of Intracellular MicroRNAs. *ACS Appl. Bio Mater.* **2021**, *4*, 1668−1676.
(43) Abeywickrama, C. S.; Wijesinghe, K. J.; Stahelin, R. V.; Pang, Y. Red-Emitting Pyrene−Benzothiazolium: Unexpected Selectivity to Lysosomes for Real-Time Cell Imaging without Alkalinizing Effect. *Chem. Commun.* **2019**, *55*, 3469−3472.
(44) Niko, Y.; Didier, P.; Mely, Y.; Konishi, G.-I.; Klymchenko, A. S. Bright and Photostable Push-Pull Pyrene Dye Visualizes Lipid Order Variation between Plasma and Intracellular Membranes. *Sci. Rep.* **2016**, *6*, 18870.
(45) Wawi, M. J.; Bijoux, A.; Inguimbert, N.; Mahler, C.; Wagner, S.; Marder, T. B.; Ribou, A. C. Peptide Vectors Carry Pyrene to Cell Organelles Allowing Real-Time Quantification of Free Radicals in Mitochondria by Time-Resolved Fluorescence Microscopy. *ChemBioChem* **2021**, *22*, 1676−1685.
(46) Cao, H.; Qi, Y.; Gao, X.; Wei, Z. J.; Xia, J.; Wang, L.; Wang, H.; Yang, Y.; Li, J. Two-Photon Excited Peptide Nanodrugs for Precise Photodynamic Therapy. *Chem. Commun.* **2021**, *57*, 2245−2248.
(47) Feng, X.; Hu, J.-Y.; Redshaw, C.; Yamato, T. Functionalization of Pyrene To Prepare Luminescent Materials—Typical Examples of Synthetic Methodology. *Chem.—Eur. J.* **2016**, *22*, 11898−11916.
(48) Cho, W.; Lee, H. J.; Choi, G.; Choi, S.; Oh, M. Dual Changes in Conformation and Optical Properties of Fluorophores within a Metal−Organic Framework during Framework Construction and Associated Sensing Event. *J. Am. Chem. Soc.* **2014**, *136*, 12201−12204.
(49) Liyana Gunawardana, V. W.; Mezei, G. Amplification of Impurity upon Complex Formation: How a 2% Ligand Impurity Lowers the Corresponding Complex Purity to 50%. *New J. Chem.* **2018**, *42*, 17195−17202.
(50) Himo, F.; Lovell, T.; Hilgraf, R.; Rostovtsev, V. V.; Noodleman, L.; Sharpless, K. B.; Fokin, V. V. Copper(I)-Catalyzed Synthesis of Azoles. DFT Study Predicts Unprecedented Reactivity and Intermediates. *J. Am. Chem. Soc.* **2005**, *127*, 210−216.
(51) Liang, L.; Astruc, D. The Copper(I)-Catalyzed Alkyne-Azide Cycloaddition (CuAAC) "Click" Reaction and Its Applications. An Overview. *Coord. Chem. Rev.* **2011**, *255*, 2933−2945.
(52) Schulze, M.; Scherer, A.; Diner, C.; Tykwinski, R. Synthesis of 1-Bromopyrene and 1-Pyrenecarbaldehyde. *Org. Synth.* **2016**, *93*, 100−114.
(53) Niamnont, N.; Kimpitak, N.; Wongravee, K.; Rashatasakhon, P.; Baldridge, K. K.; Siegel, J. S.; Sukwattanasinitt, M. Tunable Triphenylamine-based Fluorophores for Fluorescence Quenching Detection and Identification of Nitro-based Explosives. *Chem. Commun.* **2013**, *49*, 780−782.
(54) Molander, G. A. Handbook of Reagents for Organic Synthesis. *Catalyst Components for Coupling Reactions*; Wiley, 2008; pp 332−343.

https://doi.org/10.1021/acsomega.1c05619
ACS Omega 2021, 6, 33180−33191